SCITECH
RESEARCH ORGANISATION

Volume 4, Issue 2
June 11, 2018

Boson Journal of Modern Physics
www.scitecresearch.com

# The Spiral Solenoids and the Leaf Antenna in Phyllotaxis Differential Geometry

I.M.Fabbri[1]

[1]*Department of Physics, University of Milan, via Celoria 16, 20133 Milan, Italy, italomariofabbri@crfm.it*

## Abstract

In this paper new classes of spiral thin filamentary wire magnetic coils and antennas are introduced theoretically. This study shows that the thin wire circular loop coil as well as the cylindrical solenoid are particular cases of these classes. If the small spiral filamentary wire leaf loop coil is driven by an alternating electrical current, it will radiate as an antenna.

The fundamental spiral coil named leaf coil is obtained by joining together the so called *forward* and *backward* spiral coils which define the new concept of the *differential geometry of phyllotaxis*. The other spiral coils are composed of symmetrically rotated leaf coils, combined together in such a way to eliminate the transverse magnetic components along the longitudinal z axis. The magnetic moments and the multi-pole expansions of the various types of spiral loop coils are obtained by using the Taylor series of the spiral vector magnetic potentials.

According to the formulas and simulations, the magnetic flux density created by the long spiral solenoids is uniform and is equal to that created by the long cylindrical solenoid.

The bifolium coil may be flattened along one axis to meet the requirements of specific geometrical needs of space technology. Moreover, the crown solenoids may be cooled down to low temperatures by exploiting the holes in between their coils.

Applications of the spiral induction coils are countless and can be found in space technology measurements, spacecraft magnetic shielding, telemetry, telecommunication, electron optics, physics and engineering.

**Keywords:** Spiral solenoids; leaf antenna; differential geometry of phyllotaxis; magnetic coils.

## 1. Introduction

The magnetic coils never end to surprise the World with new applications and scientific discoveries. Coming from the chinese word meaning *natural energy*, the *Qi* (inductive power standard) created by the *Wireless Power Consortium (WPC)* [1] is probably the best known of the various current low power wireless charging standards that are on the current technology market. Based on the core principle of electromagnetic inductance, the charging *Qi* station contains one primary coil (TX) which creates an oscillating magnetic field capable of transferring power by inducing an alternating current in the secondary receiving coil (RX) located on the device being charged. The basic physical principle of the *resonant power transmission*, dates back to the times of *Lenz* and *Tesla* [2, 3], whereas the technology is constantly evolving in search of new coil designs and systems that enhance the magnetic energy coupling and the power transfer efficiency. A flood of electronic products with efficient cost effective wireless charging capability dedicated to telecommunication, space technology, biotelemetry systems [4], industrial and military applications, is continuously arriving on the market, driving the research on the electromagnetism of the magnetic coils and on the technology needed to optimize their operability across a very wide range of power levels. Solenoid is an old term coined back in 1820 [5] when *Ampère* showed that this coils arrangement in cylindrical geometry behaves like a bar magnet, opening up the idea of interpreting all magnetic phenomena in terms of electric currents. Since then, the cylindrical solenoids have been used in a variety of scientific applications and in almost every conceivable industrial application in the World. This pioneering introductory paper describes some of the additional theoretical benefits of the solenoids when considering *phyllotaxis patterns of leaves* in spiral differential geometry [6, 7].

As wireless technology has become increasingly accessible to the general population, the interactions of the electromagnetic fields with biological systems have stimulated the interest of the scientific community and new branches of science are born.

T*ranscranial magnetic stimulation* (TMS) [8], for example, is a non-invasive high-tech deep brain procedure involved in treatment and diagnosis of neurological disorders that makes use of short alternating magnetic fields to increase the blood flow to tissue and to stimulate cells brain nerves responsible for regulating mood, memory and decision-making, helping neurons communicate better with each other.

The spatial resolution of TMS is highly dependent upon the shape of the stimulating coil [9], accordingly the researchers are pursuing new ways to provide a precise focused physical stimulation of specific parts of the brain with advanced designs of magnetic coils, whose analysis are reported in specialized researches [10, 11].

*Magnetic Resonance Imaging* (MRI) requires a strong, highly uniform static magnetic field, known as the main field to create the initial longitudinal magnetization in the object and to maintain *Larmor's* precession of nuclear spins at constant angular frequency [12].

Spiral geometry adds flexibility in the design and fabrication of the magnetic coils, providing new efficient alternative solutions to create intense and uniform magnetic fields for MRI applications, magnetic pulses for TMS treatments and elm waves for new types of *Phyllotaxis wireless charging stations* (PWCS) and *Phyllotaxis telemetry systems* (PTS).

N*euroergonomic* technology known as IMES (*Implanted MyoElectric Sensors*) [13, 14] powered by tiny magnetic coil-antennas implanted through hypodermic needles, will allow wireless brain controlled prostheses to be widely available in the foreseeable future.

*High-sensitivity Personal Assistant Devices* (PAD) such as RF-MEMS *telemetry strain* [15] and *bio-implantable* [16] *physiological sensors* in spiral geometry, have already been proposed to monitor mechanical deformations and physiological parameters. The *differential geometry of Phyllotaxis* may allow to mock up new spiral RF-MEMS coils for magnetoinductive telemetry systems according to specific needs and to analytically study the existing spiral configurations.

Different configurations of *Phyllotaxis leaves antenna* as the *bifolium* or *crown* may be extremely efficient and useful in a wide range of applications where the design of good human-interfaces is critical.

The common shapes of the microstrip antenna [17] are circular, elliptical, square and rectangular; the spiral coordinates will allow to introduce and study analytically a new generation of 2-*dimensional Phyllotaxis patch arrays antennas* to be mounted outside aircrafts and spacecrafts.

The differential geometry of *Phyllotaxis* used to conceive new spiral loop designs with reduced

Size, Weight and Power (SWAP) could also accelerate the innovation of antenna technologies for any kind of application, including positioning, tracking and network functional devices embedded in Printed Circuit Boards (PCB) or could lead to the development of new multiple tx and rx antennas optimized for wireless MIMO systems [18].

The spacecraft induction coil magnetometers [19, 20] are used in measurement of the magnetic fields of the planets and their Van Allen's radiation belts of energy particles. With the use of the *geometry of the phyllotaxis* it is possible to conceive a new generation of magnetometers to be employed in devices for space technology such as Tri-axial Search Coil Magnetometers (SCM) [21] with *bifolium* coils.

New spiral-magnetometers and spiral coils for *Magneto-encephalography* (MEG) [23] as well as for *magnetic stimulation of the heart* [24] may be particularly sensitive and precise due to the focusing effect of their arms.

The device for the *International Thermonuclear Experimental Reactor (ITER) Programme*, a large scale scientific experiment aimed at demonstrating the viability of fusion reactions through the use of two magnetic fields -one created by electric coils, the other created by intense electric current in the plasma itself- it was conceived in toroidal geometry [25].

The greatest efforts of the researchers in the development of systems for magnetic confinement of plasma with a very high field (> 13 T), have focused on new superconducting materials [26] rather than on the exploration of new geometries.

A spiral *crown* solenoid, which creates a uniform magnetic field along the longitudinal axis, may be a valid alternative for thermonuclear experiments or in any situation where the high temperature results in an increased risk of failure of the electronic systems such as superconducting magnetic shields of spacecraft [27, 28], since the holes in between the spiral coils can allow the cooling system to be more effective than the cylindrical or toroidal case.

In various technological and scientific applications, where the uniformity of the magnetic field within a volume of interest for the development of miniaturized devices [29] is essential, the flattened *bifolium* solenoids can be exploited to improve the flexibility for free-modelling according to specific geometrical requirements.

Space technology, whose system requirements are constantly evolving toward large packaging densities with significant geometric constraints and complex configurations, could benefit from the introduction of the spiral solenoids, *e.g.* for an accurate linear control of the fluid pressure to drive pistons and valves of spacecraft according to specific optimized and reliable designs or for new magnetic shields to protect interplanetary manned spaceflights.

New maps of the nearby galaxy IC342 or Caldwell 5 [30] have recently shown that the magnetic fields in the ISM (interstellar medium) interact with its spiraling arms of gas flowing inward at its center. Since the total radio continuum emission of IC342 observed with the telescopes is not widespread but concentrated in spiral arms [30], the analysis of the power radiated by the current flowing along rotated spiral paths can be helpful to study how the magnetic fields are distributed around the galaxy in the ISM and related phenomena such as the black holes eventually housed and also the production of new stars.

Despite the interesting results that could be found by comparing the induction coils currently used with the new spiral coils, the aim of this work is to introduce an initial mathematical tool for a stepped path in the field of the coil design, are therefore required further in-depth analysis and dedicated research projects in the future.

## 2. THE SINGLE SPIRAL COIL

Magnetic fields are created by electric currents which arises due charges in motion along wires, thus the geometry of their trajectories is essential for analytical calculations. The xpressions for the magnetic flux densities $\vec{B}$ of simple planar circular current loops have been published in cartesian, cylindrical and spherical coordinates [31]. To study the spatial dependence of the magnetic field created by a steady electric current I flowing in a filamentary wire spiral coil (see Fig. **1a**), the appropriate coordinates-system [6, 7] is

$$x' = e^{\left(\frac{\delta'}{g} - g\theta'\right)} \cos\left(\delta' + \theta'\right),$$
$$y' = e^{\left(\frac{\delta'}{g} - g\theta'\right)} \sin\left(\delta' + \theta'\right), \qquad (2.1)$$
$$z' = z'.$$

where ”’” refers to the coordinates of the spiral coil as indicated in Fig. (**1a**). In the reference frame of the filamentary wire spiral coil, the trajectory of the current density $\vec{I}$ is identified by $\delta = \delta'$. The Biot-Savart law gives the magnetic flux density $\overrightarrow{dB}$ created by an infinitesimal element of the filamentary wire spiral coil $\overrightarrow{d\ell}$ (see Fig. **1a**) carrying the current I,

$$\overrightarrow{dB} = \frac{\mu_0}{4\pi} \frac{I\overrightarrow{d\ell'} \times \vec{r}}{r^3}, \qquad (2.2)$$

Where $\mu_0 = 4\pi x 10^{-7}$ is the permeability of the free space, $\overrightarrow{d\ell'} = h_\theta' d\theta' \hat{e}_\theta'$ and $h_\theta'$ is the *Lamè's* coefficient of the spiral transformation [7].

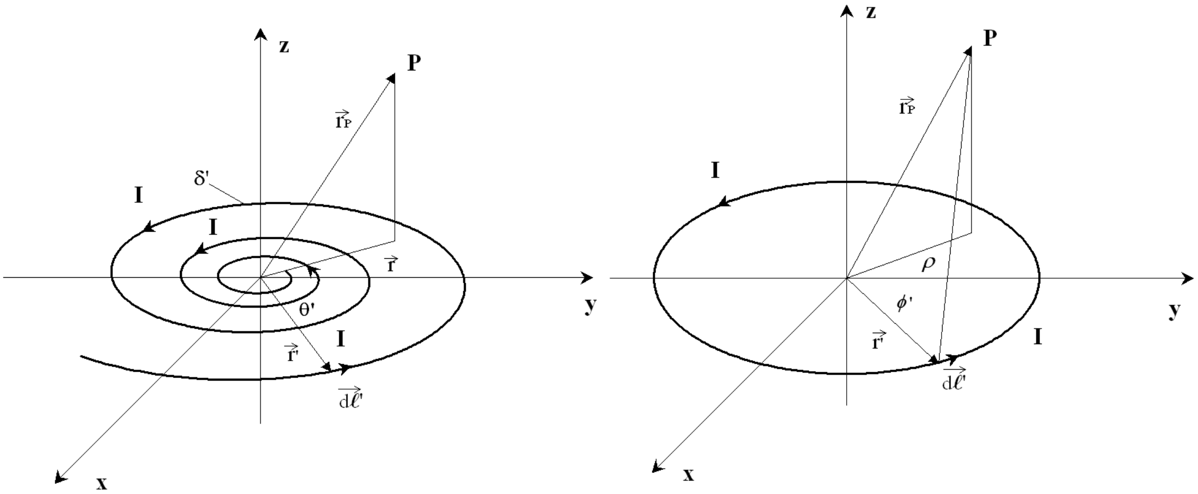

**a)** **b)**

**Fig. (1).** Perspective views of **a**) The single spiral filamentary wire coil, **b**) the circular filamentary wire coil.

In Eq. (2.2) $\vec{r} = \vec{r}_p - \vec{r}'$ the spiral coil is identified by the vector $\vec{r}'$, whereas the generic point in the space is identified by $\vec{r}_p$. According to the Eq. (2.2), the magnetic flux density in the center of the spiral coil $\vec{r}_p = 0$ is determined by

$$\vec{B}\left(\vec{r}_p = 0\right) = \frac{\mu_0 I e^{-\frac{\delta'}{g}}}{4g\pi} \left[ e^{g\theta_f'} - e^{g\theta_i'} \right] \hat{e}_z \qquad (2.3)$$

Notably, the intensity of the magnetic flux density weakens at an exponential rate with the increasing of the negative $\theta_i', \theta_f' < 0$ spiral angles, whereas it grows with the number of spiral turns $N = Int\left[\theta_f' - \theta_i'\right]$ and it can be made very high as in the particular case of the archimedean Tesla's bifilar pancake coil [3].

It is hence found that, the amount of magnetic flux density at the center of the spiral coil depends critically on the g factor.

In Fig. (**2**) the component $B_z$ at z = 0 for the two cases of the spiral and circular coils, is represented as a function of x and y.

The magnetic flux density created in a generic point of the space is given by,

$$\vec{B}(\vec{r_p}) = \frac{\mu_0 I}{4\pi} \int_{\theta_i'}^{\theta_f'} \frac{\left\{ z\left(-g\sin(\alpha') + \cos(\alpha')\right)\hat{e}_x + z\left(g\cos(\alpha') + \sin(\alpha')\right)\hat{e}_y + \left[ e^{\frac{\delta'}{g} - g\theta'} - x\left(-g\sin(\alpha') + \cos(\alpha')\right) - y\left(g\cos(\alpha') + \sin(\alpha')\right) \right]\hat{e}_z \right\}}{\left\{ \left( x - e^{\frac{\delta'}{g} - g\theta'}\cos(\alpha') \right)^2 + \left( y - e^{\frac{\delta'}{g} - g\theta'}\sin(\alpha') \right)^2 + z^2 \right\}^{\frac{3}{2}}} e^{\frac{\delta'}{g} - g\theta'} d\theta', \tag{2.4}$$

$\alpha' = \theta' + \delta'$.

This result can also be obtained by taking the curl of the magnetic vector potential $\vec{A}$ [31], so that the magnetic field is divergence free.

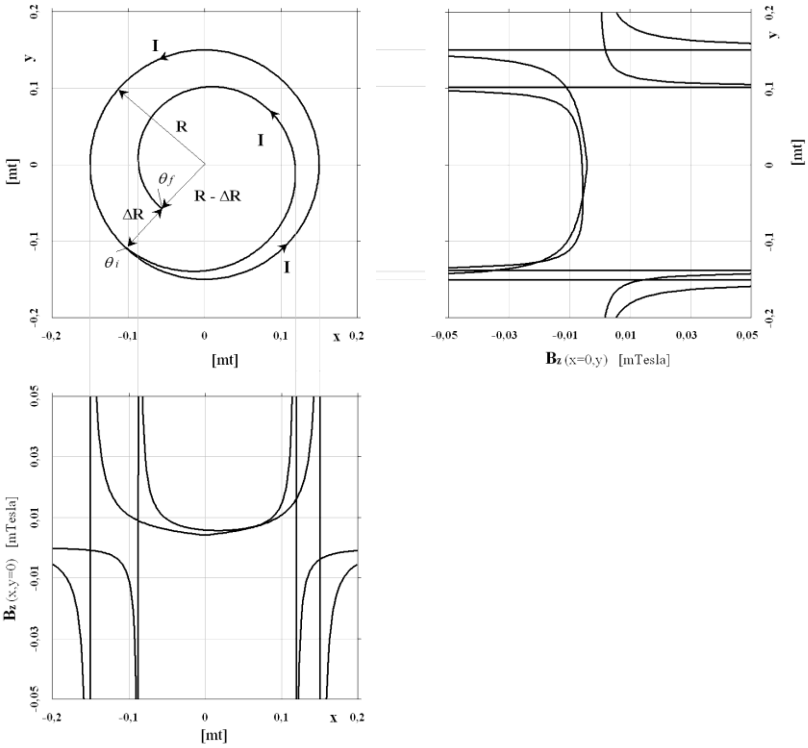

**Fig. (2a)** $B_z$ created by the spiral coil ($g$=0.1, $\delta'$=0.1) as a function of x and y variables for I = 1 (one spiral turn $\theta_i' = 28.97 rad, \theta_f' = 35.25 rad$).

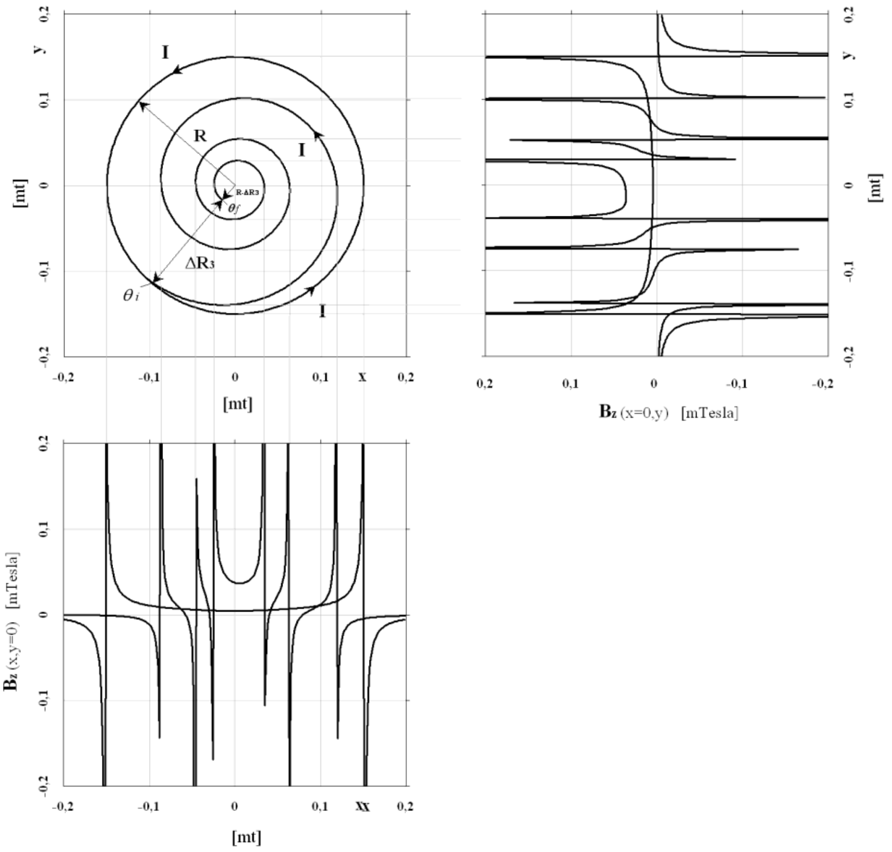

**Fig. (2b)** $B_z$ created by the spiral coil ($g$=0.1, $\delta'$=0.1) as a function of x and y variables for I = 1 (three spiral turns $\theta_i' = 28.97 rad, \theta_f' = 47.82 rad$ ).

As it can be seen in Fig. (**3**), the magnetic flux density along the z axis has three components.

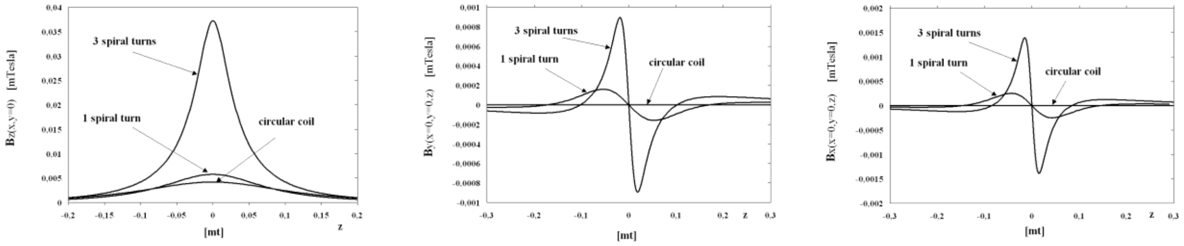

a)

b)

c)

**Fig. (3) a**) $B_z$ **b**) $B_x$ **c**) $B_y$ created by the spiral coils ($g$=0.1, $\delta'$=0.1 , one turn $\theta_i'$ =28.97 rad, $\theta_f'$ =35.25 rad and three turns $\theta_i'$ =28.97 rad, $\theta_f'$ =47.82 rad) and circular coil respectively, as a function of the z variable for I = 1A at x = 0 and y = 0.

In the particular case of the component $B_z$ (see Fig. **3a**) along the perpendicular axis z through the center of the coil, the integral of Eq. (2.4) can be evaluated analytically,

$$B_z = \frac{\mu_0 I}{4\pi g}\left[\frac{1}{\sqrt{e^{2\frac{\delta'}{g}-2g\theta'_f}+z^2}} - \frac{1}{\sqrt{e^{2\frac{\delta'}{g}-2g\theta'_i}+z^2}}\right] \tag{2.5}$$

Instead, the two components $B_x(x=0, y=0, z)$ (see Fig. **3b**) and $B_y(x=0, y=0, z)$ (see Fig. **3c**), which have the same graph along the z axis but different intensities, must be evaluated by using numerical methods.

The magnetic flux density created by a circular coil is symmetrical with respect to the z axis, whereas the single spiral coil creates a skewed field with $|B_x| > |B_y|$ (see Fig. **3b**, **c**).

The spiral multi-turn coil creates a magnetic flux density whose intensity decreases with the spiral angle θ as described in Fig. (**2b**) and has its maximum value at the center. In Table **1** a comparison between two examples of filamentary wire single spiral and circular loop coils is proposed

**Table 1. Comparison between two examples of filamentary wire single spiral and circular coils (see Figs. 1,2).**

| **Radius Circular Coil** $R = R_i$ | **Radius Increment Spiral Coil** $\Delta R$ | **g** | $\delta'$ | $\theta'_i$ [rad] | $\theta'_f$ [rad] | I [A] | **Magnetic Field Circular Coil** $B_{circle}$ $[\mu T]$ | **Magnetic Field Spiral Coil 1 Turn** $B_{spiral}$ $[\mu T]$ | **Magnetic Field Spiral Coil 3 Turn** $B_{spiral}$ $[\mu T]$ |
|---|---|---|---|---|---|---|---|---|---|
| 0.15 $m$ | 0.07 m | 0.1 | 0.1 | 28.97 | 32.254 | 1 | 4.2 | 5.7 | 37.27 |

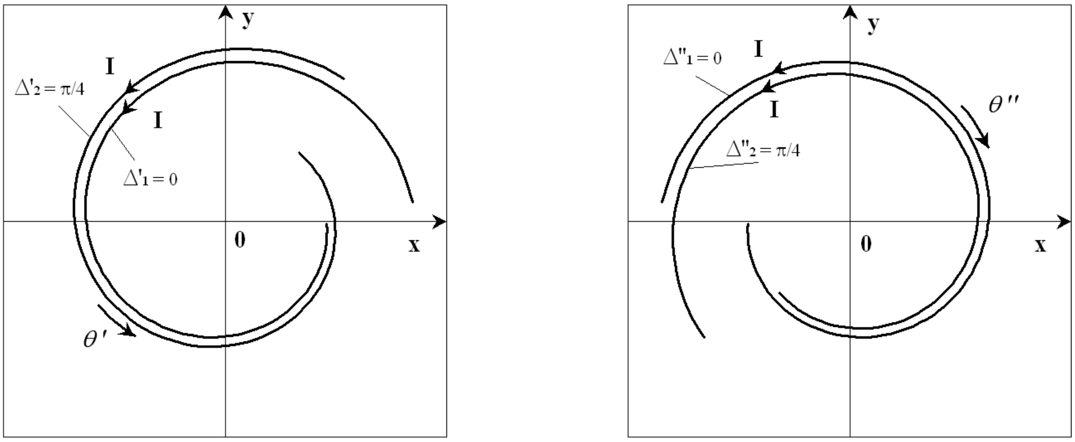

a) b)

**Fig. (4). a**) the *forward* → spiral coil clockwise rotating, **b**) *backward* ← coils counterclockwise rotating under the same matrix $[RO_{\Delta'}]_z$ increasing $\Delta'$.

## 3. *FORWARD* → AND *BACKWARD* ← SPIRAL COIL

The filamentary wire spiral coil, like the straight wire, doesn't form a closed loop.

In order to form a closed loop two types of spiral coils are considered, the *forward* spiral coil already presented in the previous section and the *backward* coil, which will be introduced afterward. Let's now rotate the reference frame coordinate system of the *forward* spiral coil in respect to the z axis by applying the rotation matrix $[RO_{\Delta'}]_z$ to the Eq. (2.1). This operation yields the following generalized forward spiral mapping

$$\begin{aligned} x' &= e^{\left(\frac{\delta'}{g}-g\theta'\right)}\cos\left(\delta'+\theta'+\Delta'\right), \\ y' &= e^{\left(\frac{\delta'}{g}-g\theta'\right)}\sin\left(\delta'+\theta'+\Delta'\right), \\ z' &= z'. \end{aligned} \qquad (3.1)$$

which has the same characteristics of the simple spiral coordinate-system of Eq. (2.1). As it can be seen in Fig. (**4**), the forward spiral coil rotates clockwise increasing $\Delta'$. While the g factor is equivalent to the angular coefficient m [7], $\Delta'$ is the analogous of the q intercept with the y axis of the straight line. On generalizing the concept, two spirals with the same g and different $\Delta_1 \neq \Delta_2$ are said to be parallel. The magnetic flux density created by the element of filamentary wire *forward* spiral coil carrying the static current I and rotated of the angle $\Delta'$ around the z axis, is given by

$$\vec{B}\left(\vec{r_p},\Delta'\right) = \frac{\mu_0 I}{4\pi}\int_{\theta_i'}^{\theta_f'} \frac{\left\{ z\left(-g\sin(\psi')+\cos(\psi')\right)\hat{e}_x + z\left(g\cos(\psi')+\sin(\psi')\right)\hat{e}_y + \left[ e^{\frac{\delta'}{g}-g\theta'} - x\left(-g\sin(\psi')+\cos(\psi')\right) - y\left(g\cos(\psi')+\sin(\psi')\right)\right]\hat{e}_z \right\} e^{\frac{\delta'}{g}-g\theta'}}{\left\{\left(x-e^{\frac{\delta'}{g}-g\theta'}\cos(\psi')\right)^2 + \left(y-e^{\frac{\delta'}{g}-g\theta'}\sin(\psi')\right)^2 + z^2\right\}^{\frac{3}{2}}}\, d\theta', \qquad (3.2)$$

$$\psi' = \theta'+\delta'+\Delta'.$$

From Eq. (3.2) and by using the principle of superposition of the effects $\vec{B}_{tot}\left(x=0,y=0,z\right) = = \vec{B}\left(x=0,y=0,z,\Delta'=0\right)+\vec{B}\left(x=0,y=0,z,\Delta'=\pi\right)$ see Fig. (5) it appears clear that two spiral filamentary wires with opposite phases create a pure longitudinal magnetic flux density along the z axis, *i.e.*

$$\vec{B}_{tot}\left(x=0,y=0,z\right) = \frac{\mu_0 I}{2\pi g}\left[\frac{1}{\sqrt{e^{2\frac{\delta'}{g}-2g\theta_f'}+z^2}} - \frac{1}{\sqrt{e^{2\frac{\delta'}{g}-2g\theta_i'}+z^2}}\right]\hat{e}_z \qquad (3.3)$$

It is worth to point out that Eq. (2.5) represents only one component of the magnetic flux density, whereas Eq. (3.3) identifies the entire magnetic vector at x = 0, y = 0 along the z axis. The reflection matrix $[RE]_{x'\to -x'}$ with respect to the y axis of the coordinate system in Eq. (2.1) and the same rotation matrix $[RO_{\Delta''}]_z$ lead to the following spiral conformal coordinates

$$\begin{aligned} x'' &= -e^{\left(\frac{\delta''}{g}-g\theta''\right)}\cos\left(\delta''+\theta''-\Delta''\right), \\ y'' &= e^{\left(\frac{\delta''}{g}-g\theta''\right)}\sin\left(\delta''+\theta''-\Delta''\right), \\ z'' &= z''. \end{aligned} \qquad (3.4)$$

where ",," refers to the coordinates of the spiral coil as indicated in Fig. (**4b**). In the spiral reference system, the equation of the backward coil is identified by the coefficient $\delta'' = \delta' = const$.

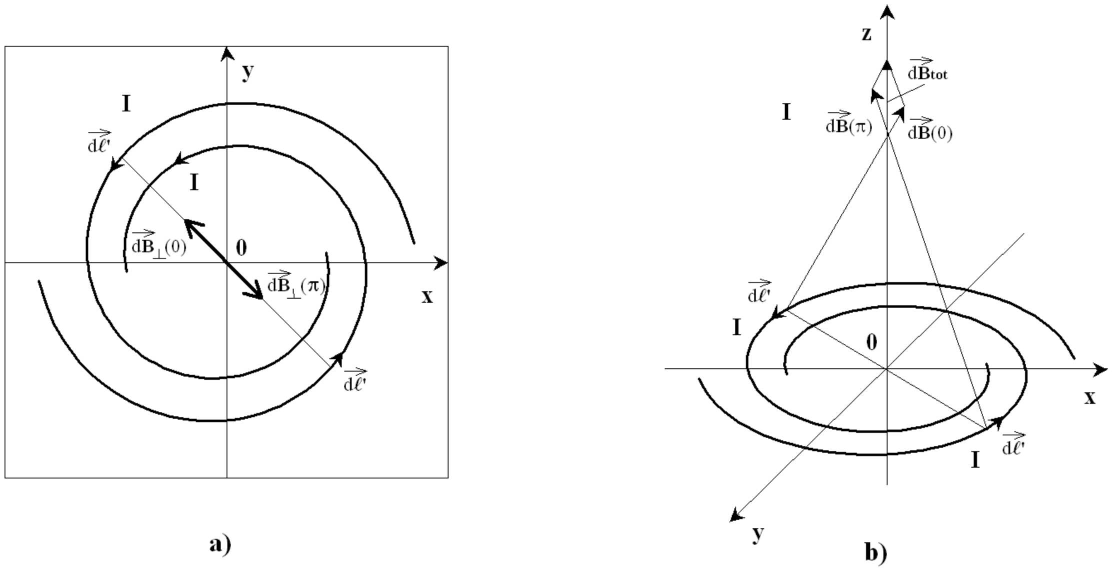

**Fig. (5).** Two spiral coils with opposite phase **a**) plane view **b**) perspective view with magnetic flux vectors.

The magnetic flux density created by the infinitesimal arc-element $\overrightarrow{d\ell''} = -h''_\theta d\theta'' \hat{e}''_\theta$ (the sign ”-” determines the direction of the current in the *backward* coil, see Fig. **4b**) of the filamentary wire *backward* spiral coil rotated by the angle $\Delta''$ and carrying the static current I, is given by

$$\vec{B}\left(\overrightarrow{r_p},\Delta''\right) = \frac{\mu_0 I}{4\pi}\int_{\theta''_i}^{\theta''_f} \frac{\left\{ z\left(-g\sin(\psi'')+\cos(\psi'')\right)\hat{e}_x + z\left(g\cos(\psi'')+\sin(\psi'')\right)\hat{e}_y + \left[ e^{\frac{\delta''}{g}-g\theta''} - x\left(-g\sin(\psi'')+\cos(\psi'')\right) + y\left(g\cos(\psi'')+\sin(\psi'')\right)\right]\hat{e}_z \right\}}{\left\{\left(x+e^{\frac{\delta''}{g}-g\theta''}\cos(\psi'')\right)^2 + \left(y-e^{\frac{\delta''}{g}-g\theta''}\sin(\psi'')\right)^2 + z^2\right\}^{\frac{3}{2}}} e^{\frac{\delta''}{g}-g\theta''}\, d\theta'', \tag{3.5}$$

$$\psi'' = \theta'' + \delta'' + \Delta''.$$

Eq. (3.2) and Eq. (3.5) differ for the sign of the arc-length element which is taken positive in the first $\theta'$ and negative $\theta''$ in the latter case (see Fig. **4**), *i.e.* the direction of the current and the direction of the angle coincide for the *forward* coil and are opposite for the *backward* one.

## 4. THE *LEAF* COIL IN *DIFFERENTIAL GEOMETRY OF PHYLLOTAXIS*

A number of coil geometries such as polar, toroidal, rectangular, *etc*. have been proposed to create different magnetic fields, but most of the spiral forms present in Nature (plants, animals, clouds, planets, stars, galaxies) have never been investigated analytically. Spiral geometry describes the mathematical characteristics of a wide range of objects found in Nature, first of all the models of botanic fingerprints such as loops and whorls or *Phyllotaxis of leaves*. Most of the spirals involved in *phyllotaxis* patterns are golden spirals or logarithmic spirals whose factor is the golden ratio $\varphi = \left(1+\sqrt{5}\right)/2$ or $g = 2\ln(\varphi)/\pi$ . Fig. (**6**) shows a new closed loop coil, called *leaf coil*, obtained from the union of the two types of open filamentary wire coils *forward* and *backward*.

The equations of the *forward* $\rightarrow$ and *backward* $\leftarrow$ coils, which form the leaf loop are

$$\begin{array}{ll}
(0)\leftarrow\begin{cases} x=-e^{\frac{\delta'}{g}-g\theta_0}\cos\left(\delta'+\theta_0-\Delta_0\right), \\ y=e^{\frac{\delta'}{g}-g\theta_0}\sin\left(\delta'+\theta_0-\Delta_0\right), \end{cases} & \begin{array}{l}\Delta_0=\Delta_1=\Delta', \qquad \delta_0=\delta_1=\delta', \\ \theta_0\in\left[-\delta'+n\pi+\dfrac{\pi}{2},-\delta'+(n+1)\pi+\dfrac{\pi}{2}\right]\end{array} \\
(1)\leftarrow\begin{cases} x=e^{\frac{\delta'}{g}-g\theta_1}\cos\left(\delta'+\theta_1+\Delta_1\right), \\ y=e^{\frac{\delta'}{g}-g\theta_1}\sin\left(\delta'+\theta_1+\Delta_1\right), \end{cases} & \theta_1\in\left[-\delta'+n\pi+\dfrac{\pi}{2},-\delta'+(n+1)\pi+\dfrac{\pi}{2}\right]
\end{array} \tag{4.1}$$

where (0), (1), are the two subsets of the plane $\mathbb{R}^2$ that represent the boundaries of the $n^{th}$ *leaf* coil. The *leaf* coordinates of Eq. (4.1) together with their basis vectors can be considered a reference point of the *differential geometry of phyllotaxis*, or the geometry of the arrangements of the leaves in the plants. The scheme of the square loop coil [32] is now taken into account in the calculation of the magnetic flux density created by the $n^{th}$ *leaf* coil loop. According to Eq. (3.2) and Eq. (3.5), it follows

$$\vec{B}_n\left(\vec{r_p},\delta'=\delta'',\Delta',\circlearrowleft\uparrow\right)=\vec{B}_n\left(\vec{r_p},\Delta',\rightarrow\right)+\vec{B}_n\left(\vec{r_p},-\Delta',\leftarrow\right)=$$

$$=\frac{\mu_0 I}{4\pi}\sum_{k=0}^{1}\int_{-\delta'+n\pi+\frac{\pi}{2}}^{-\delta'+(n+1)\pi+\frac{\pi}{2}}\frac{\left\{(-1)^{k+1}z\left(-g\sin(\psi_k)+\cos(\psi_k)\right)\hat{e}_x+z\left(g\cos(\psi_k)+\sin(\psi_k)\right)\hat{e}_y+\left[e^{\frac{\delta'}{g}-g\theta_k}+(-1)^k x\left(-g\sin(\psi_k)+\cos(\psi_k)\right)-y\left(g\cos(\psi_k)+\sin(\psi_k)\right)\right]\hat{e}_z\right\}}{\left\{\left(x+(-1)^k e^{\frac{\delta'}{g}-g\theta_k}\cos(\psi_k)\right)^2+\left(y-e^{\frac{\delta'}{g}-g\theta_k}\sin(\psi_k)\right)^2+z^2\right\}^{\frac{3}{2}}}e^{\frac{\delta'}{g}-g\theta_k}d\theta_k,$$

$$\psi_k=\theta_k+\delta''+(-1)^{k+1}\Delta'. \tag{4.2}$$

According to eq. (4.2), for $x=0,y=0,\Delta'=0$, the magnetic flux density x-component created by the $n^{th}$ leaf (see Fig. 7) along the axis z is $B_{x_n}=0$, whereas $B_{z_n},B_{y_n}\neq 0$.

Particularly

$$B_{z_n}\left(x=0,y=0,z,\Delta'=0\right)=\frac{\mu_0 I}{2\pi g}\left[\frac{1}{\sqrt{e^{2\frac{\delta'\left(1+g^2\right)}{g}-2g\left(n+\frac{3}{2}\right)\pi}+z^2}}-\frac{1}{\sqrt{e^{2\frac{\delta'\left(1+g^2\right)}{g}-2g\left(n+\frac{1}{2}\right)\pi}+z^2}}\right] \tag{4.3}$$

### 4.1. The *leaf* Multipole Magnetic Moment Expansion

Taking into account the properties of a filamentary wire *leaf* loop current distribution which is localized in a small region of space, it is possible to expand the vector magnetic potential in multipoles. For the distribution of the steady-state currents in the idealized filamentary zero thickness wire of the closed *leaf* loop, the vector potentials have the expansion [31,33]

$$A_j(x,y,z)=\frac{\mu_0}{4\pi}\int\frac{J_i\left(\vec{r'}\right)d^3r'}{\left|\vec{r_p}-\vec{r'}\right|}=\frac{\mu_0 I}{4\pi}\left[\frac{1}{\left|\vec{r_p}\right|}\int J_i\left(\vec{r'}\right)d^3r'+\vec{r_p}\bullet\int J_i\left(\vec{r'}\right)\vec{r'}d^3r'+......\right], \qquad j\equiv x,y,z. \tag{4.4}$$

where,

$$\vec{J}\left(\vec{r'}\right)d^3r'\equiv I\begin{cases}\overrightarrow{d\ell'}\rightarrow \textit{forward coil} \\ -\overrightarrow{d\ell'}\rightarrow \textit{backward coil.}\end{cases} \tag{4.5}$$

Since the first integral in eq. (4.4) is only the total displacement of the vector around a closed loop, the *leaf* monopole term vanishes.

For $\left|\vec{r}_p\right| \gg \left|\vec{r}\,'\right|$ , the multipole moment expansion will be dominated by the non-vanishing multipole of a lowest-order; terms of higher-order in the expansion can be neglected. The first lowest nonvanishing term in the expansion of the vector magnetic potential of the *leaf* loop $\vec{A}$ can be expressed in term of the magnetic moment $\vec{\mu}_{(1),M}$ of the current distribution $\vec{J}$, *i.e.*

$$\vec{A} \simeq \frac{\mu_0}{4\pi} \frac{\vec{\mu}_{(1),M} \times \vec{r}_p}{\left|\vec{r}_p\right|^3}, \tag{4.6}$$

where,

$$\begin{aligned} \vec{\mu}_{(1),M} &= \frac{I}{2} \oint\limits_{leaf\ \ loop} \vec{d\ell}\,' \times \vec{r}\,' = I \sum_{n=n_0}^{M} S_{(1)_n} \hat{e}_z, \\ S_{(1)_n} &= \frac{e^{\left(2\frac{\delta'\left(1+g^2\right)}{g} - 2g\left(n+\frac{1}{2}\right)\pi\right)}}{2g}\left[1 - e^{-2gn\pi}\right]. \end{aligned} \tag{4.7}$$

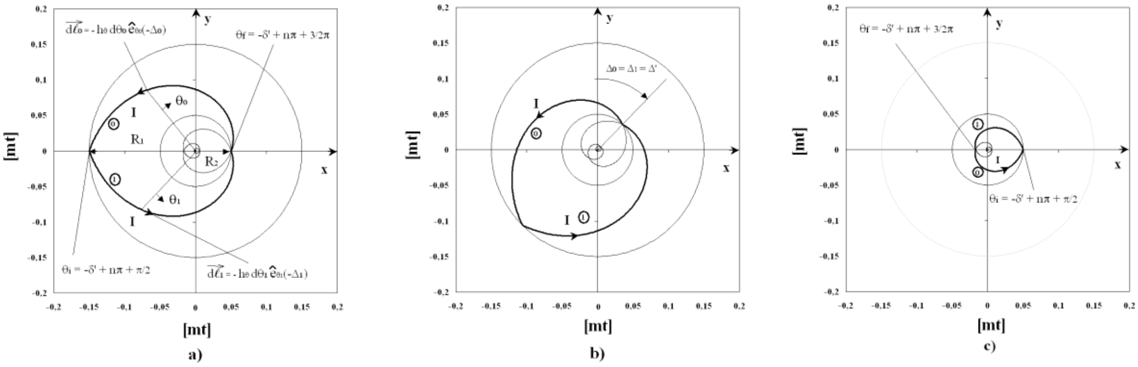

**Fig. (6).** Leaf coil for $n=1, g=0.35, \delta' = -0.07765, R_1 = 0.15mt, R_2 = 0.05mt, \delta_0 = \delta_1 = \delta_2$ .
**a)** $n=1, \Delta_0 = \Delta_1 = \Delta' = -\pi/2$ **b)** rotated by $n=1, \Delta_0 = \Delta_1 = \Delta' = -\pi/4$ , **c)** $n=2, \Delta_0 = \Delta_1 = \Delta' = -\pi/2$ .

Where $S_{(1)_n}$ is the total area of the $n^{th}$ *leaf* loop (the number $"(1) \equiv 2^{N=0}"$ identifies the leaf type of coil). Since $M \in \mathbb{Z}$ in eq. (4.7), the magnetic moment of the *multileaf* coil is quantized (see Fig. 8) and $\vec{\mu}_{(1),n_0}$ represents the fundamental magnetic moment of the *multileaf* coil.

For $\left|\vec{r}_p\right| \ll \left|\vec{r}\,'\right|$, the vector potential of the multileaf loop $\vec{A}$ is expressed following the power Taylor series

$$\vec{A} = \frac{\mu_0}{4\pi} \sum_{n=0}^{\infty} \frac{1}{\left|\vec{r}_p\right|^{n+1}} \oint\limits_{leaf\ \ loop} \left|\vec{r}\,'\right|^n P_n\left(\frac{\vec{r}_p \bullet \vec{r}\,'}{\left|\vec{r}_p\right|\left|\vec{r}\,'\right|}\right) \vec{d\ell}\,' \tag{4.8}$$

Where $P_n$ are ordinary Legendre polynomial of $1^{st}$ kind of order n. The first term $\left(\sim 1/\left|\vec{r}_p\right|\right)$ in the expansion of eq. (4.8) is the magnetic monopole term, the $2^{nd}$ term $\left(\sim 1/\left|\vec{r}_p\right|^2\right)$ is the magnetic dipole term, the $3^{nd}$ term $\left(\sim 1/\left|\vec{r}_p\right|^3\right)$ is the magnetic quadrupole term, and so on.

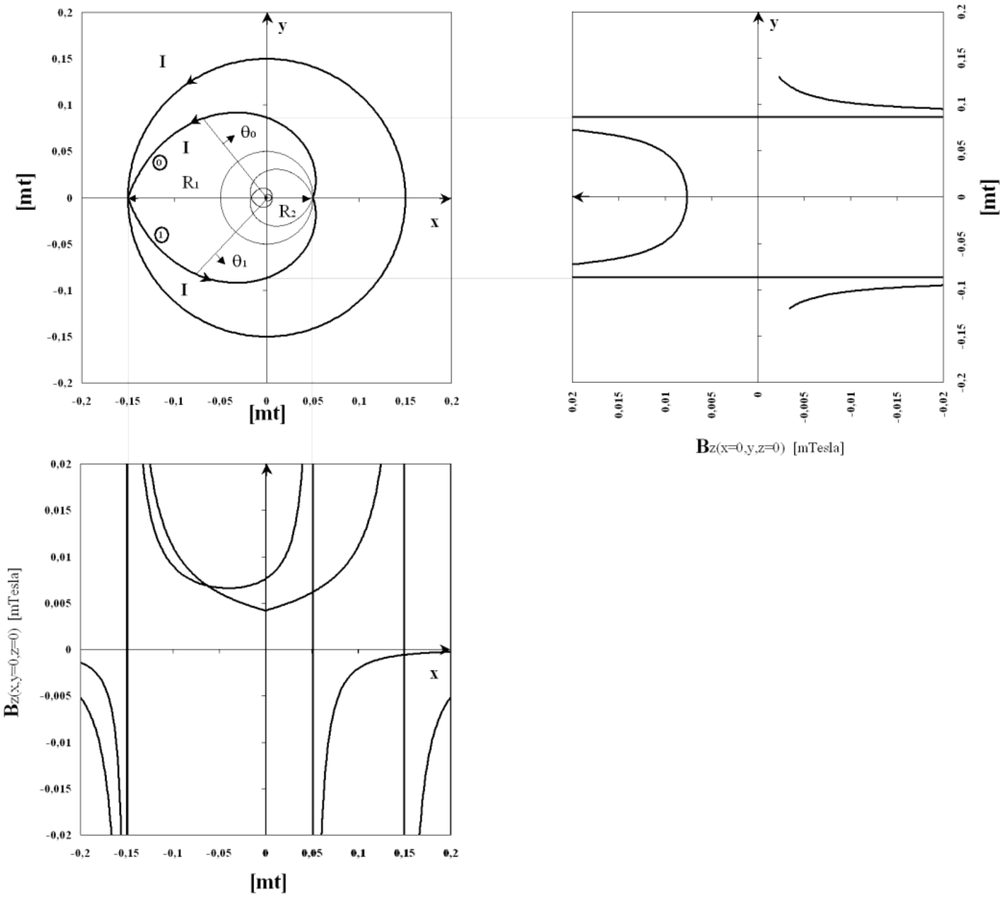

**Fig. (7).** $B_z$ as a function of x at y = 0 and as a function of y at $x=0, y=0, \Delta=-\pi/2$, for $g=0.35, \delta'=-0.0765, n=1$.

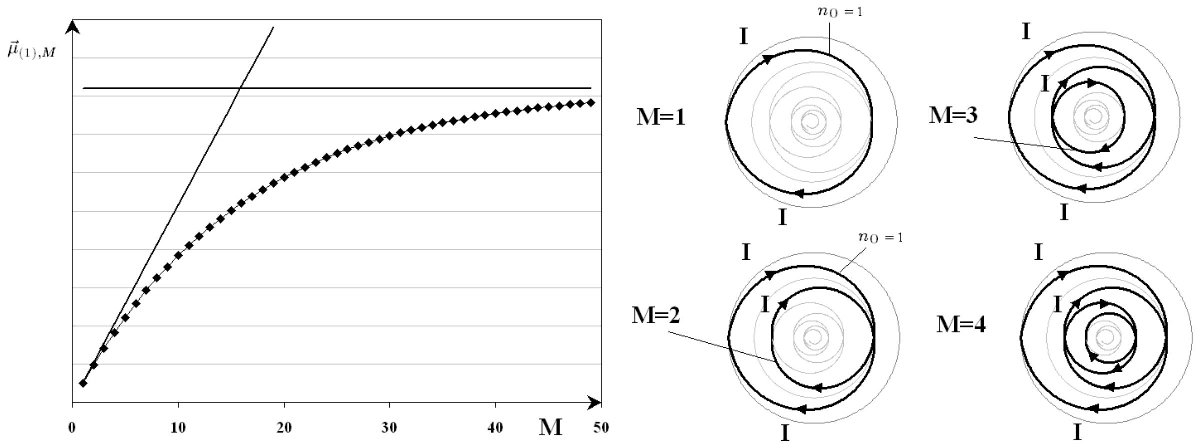

**Fig. (8).** (**a**) Magnetic moment $\vec{\mu}_{(1),M}$ of (**b**) M superimposed concentric *leaf* loop coils.

## 5. THE *PHYLLOTAXIS LEAF* ANTENNA

The purpose of this section is to show how the filamentary wire leaf loop configuration radiates. Let's suppose an alternating harmonic current is driven around the $n^{th}$ filamentary wire *leaf* loop

$$I = I_0 \cos(\omega t). \tag{5.1}$$

Because of the superposition principle, the retarded potential results in [31, 33]

$$\begin{gathered}
\vec{A}(x,y,z,t)=\sum_{n=n_0}^{N}\vec{A}_{(1)_n}(x,y,z,t),\\
\vec{A}_{(1)_n}(x,y,z,t)=\frac{\mu_0 I}{4\pi}\oint\limits_{n^{th}loop}\frac{\cos\left(\omega\left(t-\frac{r}{c}\right)\right)}{r}\overrightarrow{d\ell'}
\end{gathered}\tag{5.2}$$

Where $r=\left|\vec{r_p}-\vec{r}'\right|$ is the distance from the field (observation) point $\vec{r_p}$ to the source point $\vec{r}'$ of the *leaf* coil

$$\begin{gathered}
r=\left|\vec{r_p}-\vec{r}'\right|=\begin{cases}\sqrt{R^2+e^{\left(2\frac{\delta'}{g}-2g\theta_0\right)}+2Re^{\left(\frac{\delta'}{g}-g\theta_0\right)}\sin(\theta)\cos(\Delta')}, \\ \sqrt{R^2+e^{\left(2\frac{\delta'}{g}-2g\theta_1\right)}-2Re^{\left(\frac{\delta'}{g}-g\theta_1\right)}\sin(\theta)\cos(\Delta')}\end{cases}\\
\overrightarrow{d\ell'}=\begin{cases}-h_\theta\hat{e}_\theta''(\Delta')d\theta_0,\\ h_\theta\hat{e}_\theta''(\Delta')d\theta_1\end{cases}\qquad \theta_{0,1}\in L_n\equiv\left[-\delta'+n\pi+\frac{\pi}{2},-\delta'+(n+1)\pi+\frac{\pi}{2}\right],\\
R=\sqrt{x^2+y^2+z^2}.
\end{gathered}\tag{5.3}$$

The far-field approximation assumes that the field point r is very far from the current source [33], $R\gg e^{\left(\frac{\delta'}{g}-g\theta_0\right)},e^{\left(\frac{\delta'}{g}-g\theta_1\right)},\forall\theta_{0,1}\in L_n$. It is further assumed the size of the dipole is small compared to the wavelength of the radiation radiated [33], i.e. $e^{\left(\frac{\delta'}{g}-g\theta_0\right)},e^{\left(\frac{\delta'}{g}-g\theta_1\right)}\ll\lambda,\forall\theta_{0,1}\in L_n$. In the radiation zone $R\gg\lambda$, the first term of the vector potential $A_{(1)_n}$ is negligible, consequently the fields result in

$$\vec{E}_{(1)_n}(R,\theta,t)\simeq-\frac{\mu_0 I_0}{8\pi}\frac{\omega^2}{c}e^{\left(2\frac{\delta'\left(1+g^2\right)}{g}-2g\left(n+\frac{1}{2}\right)\pi\right)}\frac{1-e^{-2g\pi}}{g}\frac{\sin\theta}{R}\cos\left(\omega\left(t-\frac{r}{c}\right)\right)\hat{e}_\phi.\tag{5.4}$$

$$\vec{B}_{(1)_n}(R,\theta,t)\simeq\frac{\mu_0 I_0}{8\pi}\frac{\omega^2}{c^2}e^{\left(2\frac{\delta'\left(1+g^2\right)}{g}-2g\left(n+\frac{1}{2}\right)\pi\right)}\frac{1-e^{-2g\pi}}{g}\frac{\sin\theta}{R}\cos\left(\omega\left(t-\frac{r}{c}\right)\right)\hat{e}_\theta.\tag{5.5}$$

Where $\hat{e}_\theta,\hat{e}_\phi,\hat{e}_r$ are the unit spherical basis vectors [33]. These fields far from the loop are in phase, mutually perpendicular, and transverse to the direction of propagation $\hat{e}_r$ and the ratio of their amplitudes is $E_{0_n}/B_{0_n}=c$, as expected for electromagnetic waves [31, 33]. The energy flux for magnetic dipole radiation is

$$\vec{S}_{(1)_n}(R,\theta,t)=\frac{1}{\mu_0}\left(\vec{E}_{(1)_n}\times\vec{B}_{(1)_n}\right)\simeq-\frac{\mu_0}{c}\left(\frac{I_0}{8\pi}\frac{\omega^2}{c^2}e^{\left(2\frac{\delta'\left(1+g^2\right)}{g}-2g\left(n+\frac{1}{2}\right)\pi\right)}\frac{1-e^{-2g\pi}}{g}\frac{\sin(\theta)}{R}\cos\left[\omega\left(t-\frac{r}{c}\right)\right]\right)^2\hat{e}_r,\tag{5.6}$$

On averaging the intensity over the time, the lines of Poynting flux are almost purely radial once

$$\left\langle \vec{S}_{(1)_n} \right\rangle = -\left( \frac{\mu_0 I_0^2}{128\pi^2} \frac{\omega^4}{c^3} e^{\left(4\frac{\delta'\left(1+g^2\right)}{g} - 4g\left(n+\frac{1}{2}\right)\pi\right)} \frac{\left(1-e^{-2g\pi}\right)^2}{g^2} \frac{\sin^2(\theta)}{R^2} \hat{e}_r \right), \tag{5.7}$$

And the total time-average radiated power by the $n^{th}$ *leaf* loop antenna, is

$$\left\langle \vec{P}_{(1)_n} \right\rangle = -\left( \frac{\mu_0 I_0^2}{48\pi^2} \frac{\omega^4}{c^3} e^{\left(4\frac{\delta'\left(1+g^2\right)}{g} - 4g\left(n+\frac{1}{2}\right)\pi\right)} \frac{\left(1-e^{-2g\pi}\right)^2}{g^2} \right). \tag{5.8}$$

The signs “-“ in eq. (5.8) and eq. (5.7) depend on the orientation of the *leaf* loop coil, which point in the –x direction (see Fig. 7). The total power radiated by the superposition of infinite concentric *leaf* dipole antennas is

$$P(\omega) = \frac{\left\langle \vec{P}_{(1)n_0} \right\rangle e^{4g\pi}}{e^{(4g\pi)} - 1}, \qquad g > 0. \tag{5.9}$$

## 6. THE *BIFOLIUM* COIL.

The closed loop coil called *bifolium* coil of Fig. (**9**) derives from the union of two *leaf* coils, one rotated with respect to the other by an angle $\pi$.

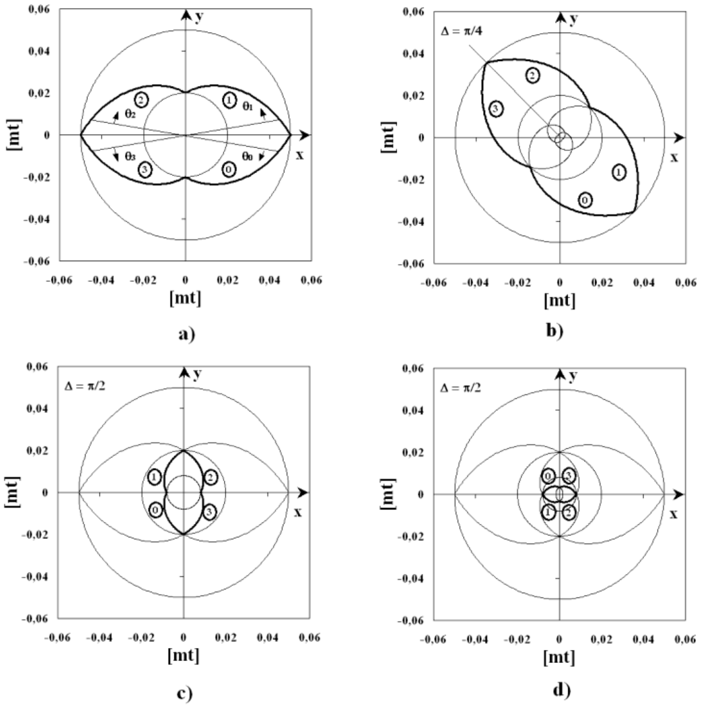

a)
b)
c)
d)

**Fig. (9).** The bifolium coil for $n=1, q=0, g=0.583, \delta'=-0.10744$ **a)** $\Delta'=\pi/2$, $R^i_{(2)}=0.05mt$, $R^f_{(2)}=0.02mt$ **b)** $\Delta'=\pi/4$, **c)** $\mathrm{n}=1,\ \mathrm{q}=1, \Delta'=\pi/2$, $R^i_{(2)}=0.02mt$, $R^f_{(2)}=0.008mt$, **d)** $\mathrm{n}=2,\ \mathrm{q}=0, \Delta'=\pi/2$, $R^i_{(2)}=0.0032mt$, $R^f_{(2)}=0.02mt$.

The equations of the *forward* → and *backward* ← coil parts are

$$
(2k)\leftarrow\begin{cases} x=-e^{\frac{\delta'}{g}-g\theta_{2k}}\cos\left(\delta'+\theta_{2k}-\Delta'-\dfrac{k\varepsilon_k\pi}{2}\right), \\ y=e^{\frac{\delta'}{g}-g\theta_{2k}}\sin\left(\delta'+\theta_{2k}-\Delta'-\dfrac{k\varepsilon_k\pi}{2}\right), \end{cases}\quad \theta_{2k}\in\left[-\delta'+n\pi+\frac{\pi}{2}+q\frac{\pi}{2},-\delta'+(n+1)\pi+\frac{\pi}{2}+q\frac{\pi}{2}\right],
$$

$$
(2k+1)\leftarrow\begin{cases} x=e^{\frac{\delta'}{g}-g\theta_{2k+1}}\cos\left(\delta'+\theta_{2k+1}+\Delta'+\dfrac{k\varepsilon_k\pi}{2}\right), \\ y=e^{\frac{\delta'}{g}-g\theta_{2k+1}}\sin\left(\delta'+\theta_{2k+1}+\Delta'+\dfrac{k\varepsilon_k\pi}{2}\right), \end{cases}\quad \theta_{2k+1}\in\left[-\delta'+n\pi+\frac{\pi}{2}+q\frac{\pi}{2},-\delta'+(n+1)\pi+\frac{\pi}{2}+q\frac{\pi}{2}\right],
$$

$$
k=0,1,q=0,1,
$$

$$
\varepsilon_k=\begin{cases}0 & k=0,\\ 1 & k\neq 0.\end{cases}
$$

(6.1)

where (2k) and (2k+1), are subset of the plane $\mathbb{R}^2$ that represent the boundaries of the $n^{th}$ *bifolium* coil.

The magnetic flux created by the *bifolium* coil which carries a static current I is given by the sum of the components *forward* and *backward*

$$
\vec{B}_{(2)_{n,q}}\left(\overrightarrow{r_p},\delta'=\delta'',\Delta',\circlearrowleft_{\uparrow}\right)=\vec{B}_{(2)_{n,q}}\left(\overrightarrow{r_p},\Delta',\rightarrow\right)+\vec{B}_{(2)_{n,q}}\left(\overrightarrow{r_p},-\Delta',\leftarrow\right)=
$$

$$
=\frac{\mu_0 I}{4\pi}\sum_{k=0}^{1}\int_{-\delta'+n\pi+(q+1)\frac{\pi}{2}}^{-\delta'+(n+1)\pi+q\frac{\pi}{2}}\frac{\left\{\begin{array}{l} z\left(-g\sin\left(\psi_k^+\right)+\cos\left(\psi_k^+\right)\right)\hat{e}_x+z\left(g\cos\left(\psi_k^+\right)+\sin\left(\psi_k^+\right)\right)\hat{e}_y+\\ +\left[e^{\frac{\delta'}{g}-g\theta_{2k+1}}-x\left(-g\sin\left(\psi_k^+\right)+\cos\left(\psi_k^+\right)\right)-y\left(g\cos\left(\psi_k^+\right)+\sin\left(\psi_k^+\right)\right)\right]\hat{e}_z\end{array}\right\}}{\left\{\left(x-e^{\frac{\delta'}{g}-g\theta_{2k+1}}\cos\left(\psi_k^+\right)\right)^2+\left(y-e^{\frac{\delta'}{g}-g\theta_{2k+1}}\sin\left(\psi_k^+\right)\right)^2+z^2\right\}^{\frac{3}{2}}}e^{\frac{\delta'}{g}-g\theta_{2k+1}}d\theta_{2k+1}+
$$

$$
+\frac{\mu_0 I}{4\pi}\sum_{k=0}^{1}\int_{-\delta'+n\pi+(q+1)\frac{\pi}{2}}^{-\delta'+(n+1)\pi+q\frac{\pi}{2}}\frac{\left\{\begin{array}{l} z\left(g\sin\left(\psi_k^-\right)-\cos\left(\psi_k^-\right)\right)\hat{e}_x+z\left(g\cos\left(\psi_k^-\right)+\sin\left(\psi_k^-\right)\right)\hat{e}_y+\\ +\left[e^{\frac{\delta'}{g}-g\theta_{2k}}+x\left(-g\sin\left(\psi_k^-\right)+\cos\left(\psi_k^-\right)\right)-y\left(g\cos\left(\psi_k^-\right)+\sin\left(\psi_k^-\right)\right)\right]\hat{e}_z\end{array}\right\}}{\left\{\left(x+e^{\frac{\delta'}{g}-g\theta_{2k}}\cos\left(\psi_k^-\right)\right)^2+\left(y-e^{\frac{\delta'}{g}-g\theta_{2k}}\sin\left(\psi_k^-\right)\right)^2+z^2\right\}^{\frac{3}{2}}}e^{\frac{\delta'}{g}-g\theta_{2k}}d\theta_{2k},
$$

$$
\psi_k^+=\delta'+\theta_{2k+1}+\Delta'+\frac{k\varepsilon_k\pi}{2},
$$

$$
\psi_k^-=\delta'+\theta_{2k}-\Delta'-\frac{k\varepsilon_k\pi}{2},
$$

$$
k=0,1,q=0,1.
$$

(6.2)

According to Eq. (6.2), for x = 0, y = 0 the magnetic flux density x-y-components created by the *bifolium* coil along the axis $z\neq 0$ are $B_{(2)_{x,n,q}}=0, B_{(2)_{y,n,q}}=0,$ and (see Fig. **10**)

$$
B_{(2)z_{n,q}}(x=0,y=0,z)=\frac{\mu_0 I}{\pi g}\left[\frac{1}{\sqrt{e^{2\frac{\delta'\left(1+g^2\right)}{g}-2g(n+1)\pi-qg\pi}+z^2}}-\frac{1}{\sqrt{e^{2\frac{\delta'\left(1+g^2\right)}{g}-2g\left(n+\frac{1}{2}\right)\pi-qg\pi}+z^2}}\right]
$$

(6.3)

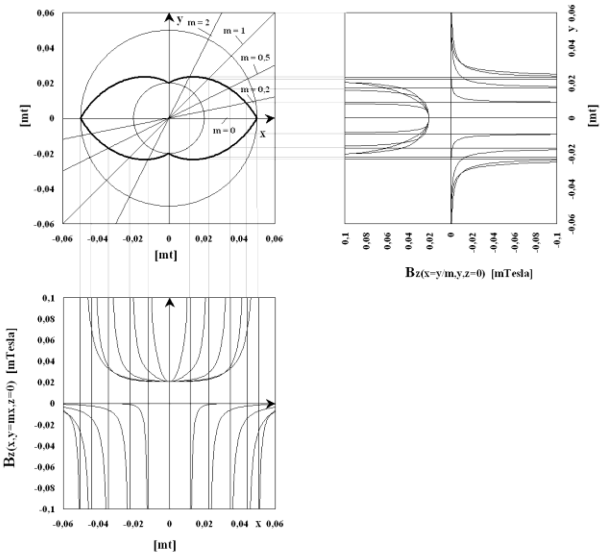

**Fig. (10).** $B_{(2)z_{n,q}}$ of the bifolium coil $(n=1, q=0)$ as a function of x, y = mx, and y, $x = y/m$ for $g = 0.583, \delta' = -0.10744$, $R^{i}_{(2)} = 0.05mt$, $R^{f}_{(2)} = 0.02mt$, $\Delta' = \pi/2$, m = 0, 0.2, 0.5, 1, 2.

The magnetic flux density of the *bifolium* around the axis y has no the $B_x$ component, whereas the circular coil creates a symmetrical transverse field $B_\rho$ .

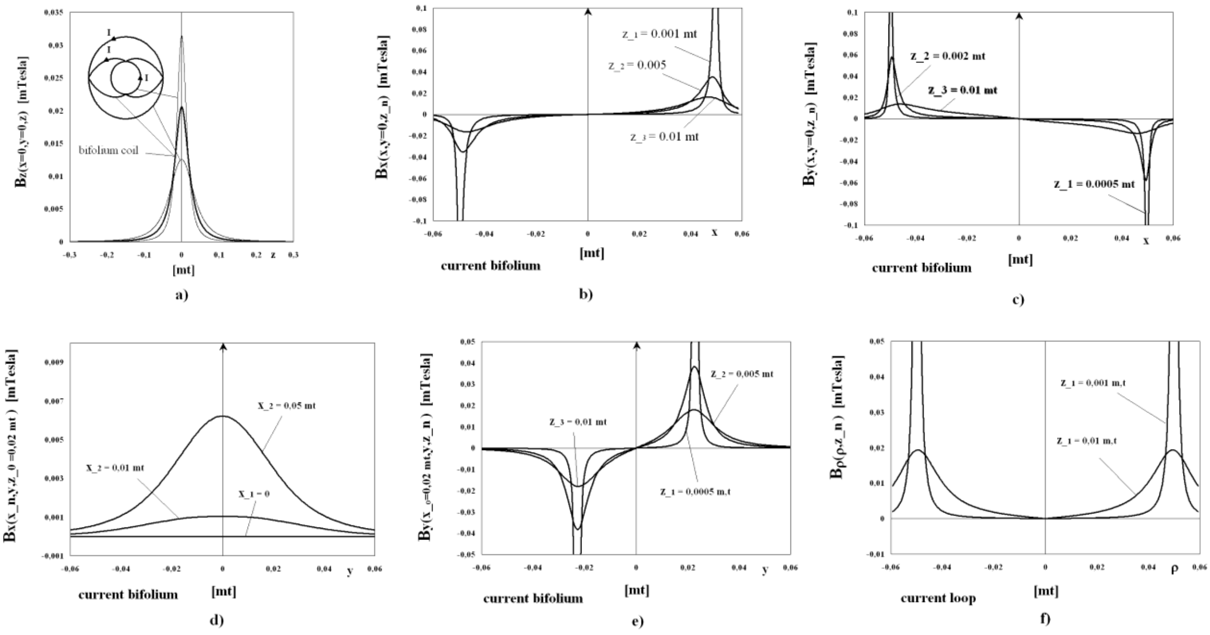

**Fig. (11).** bifolium coil with for g=0.5833, $\delta' = -0.10744$, $n$=1, $R^{i}_{(2)} = 0.05mt, R^{f}_{(2)} = 0.05mt$ , $\Delta' = \pi/2$, circular coil with $r_1' = 0.05mt$ and $r_2' = 0.02mt$ **a)** $B_z$ as a function of z at the center of the coils $x = 0, y = 0$ and comparison between circular and *bifolium* coils, **b), c)** $B_x, B_y$ as a function of x at $y = 0$ of the *bifolium* coil, **d), e)** $B_x, B_y$ , as a function of y of the *bifolium* coil **f)** $B_\rho$ as a function of $\rho$ at different value of z for the circular loop coil $r_1' = 0.05mt$ .

## 7. THE *BIFOLIUM* SOLENOID.

The magnetic field of an ideal solenoid *bifolium* can be derived from the Biot-Savart law [34].

$$\vec{B}\left(\vec{r_p}\right)=\int_{-\frac{L}{2}}^{\frac{L}{2}}\frac{\mu_0}{4\pi}\oint_{leaf\ \ loop}\frac{I\left(\mathbb{N}dz\right)\overrightarrow{d\ell'}\times\vec{r}}{\left|\vec{r}\right|^3}. \tag{7.1}$$

where $r=\left|\vec{r_p}-\vec{r}'\right|$ .

Exactly as for the circular coil, the axial magnetic field of a *bifolium* loop carrying the static current I has no transversal components. To find the magnetic field due to a finite *bifolium* solenoid, we will have to approximate the solenoid as constituted by a large number of close *bifolium* loops.

Let's take a packed *bifolium* loops located at z with a thickness $dz'$, as shown in Fig. (**12**), the amount of current flowing through it is proportional to $dz'$ and is given by $dI=I\left(\mathbb{N}dz'\right)$, where $\mathbb{N}=N/L$ is the number of turns $N$ per unit length $L$. According to Eq. (6.2) and Eq. (7.1), the magnetic flux density created by the *bifolium* solenoid is given by

$$\begin{aligned}
&\vec{B}(2)_{sol,n,q}\left(\vec{r_p},\delta'=\delta'',\Delta',\bigcirc_{\uparrow}\right)=\vec{B}(2)_{sol,n,q}\left(\vec{r_p},\Delta',\rightarrow\right)+\vec{B}(2)_{sol,n,q}\left(\vec{r_p},-\Delta',\leftarrow\right)=\\
&=\frac{\mu_0 I}{4\pi}\sum_{k=0}^{1}\int_{-\frac{L}{2}}^{\frac{L}{2}}\mathbb{N}dz'\int_{-\delta'+n\pi+(q+1)\frac{\pi}{2}}^{-\delta'+(n+1)\pi+q\frac{\pi}{2}}\frac{\left\{\begin{array}{l}(z-z')\left(-g\sin\left(\psi_k^+\right)+\cos\left(\psi_k^+\right)\right)\hat{e}_x+(z-z')\left(g\cos\left(\psi_k^+\right)+\sin\left(\psi_k^+\right)\right)\hat{e}_y+\\+\left[e^{\frac{\delta'}{g}-g\theta_{2k+1}}-x\left(-g\sin\left(\psi_k^+\right)+\cos\left(\psi_k^+\right)\right)-y\left(g\cos\left(\psi_k^+\right)+\sin\left(\psi_k^+\right)\right)\right]\hat{e}_z\end{array}\right\}}{\left\{\left(x-e^{\frac{\delta'}{g}-g\theta_{2k+1}}\cos\left(\psi_k^+\right)\right)^2+\left(y-e^{\frac{\delta'}{g}-g\theta_{2k+1}}\sin\left(\psi_k^+\right)\right)^2+\left(z-z'\right)^2\right\}^{\frac{3}{2}}}e^{\frac{\delta'}{g}-g\theta_{2k+1}}d\theta_{2k+1}+\\
&+\frac{\mu_0 I}{4\pi}\sum_{k=0}^{1}\int_{-\frac{L}{2}}^{\frac{L}{2}}\mathbb{N}dz'\int_{-\delta'+n\pi+(q+1)\frac{\pi}{2}}^{-\delta'+(n+1)\pi+q\frac{\pi}{2}}\frac{\left\{\begin{array}{l}(z-z')\left(g\sin\left(\psi_k^-\right)-\cos\left(\psi_k^-\right)\right)\hat{e}_x+(z-z')\left(g\cos\left(\psi_k^-\right)+\sin\left(\psi_k^-\right)\right)\hat{e}_y+\\+\left[e^{\frac{\delta'}{g}-g\theta_{2k}}+x\left(-g\sin\left(\psi_k^-\right)+\cos\left(\psi_k^-\right)\right)-y\left(g\cos\left(\psi_k^-\right)+\sin\left(\psi_k^-\right)\right)\right]\hat{e}_z\end{array}\right\}}{\left\{\left(x+e^{\frac{\delta'}{g}-g\theta_{2k}}\cos\left(\psi_k^-\right)\right)^2+\left(y-e^{\frac{\delta'}{g}-g\theta_{2k}}\sin\left(\psi_k^-\right)\right)^2+\left(z-z'\right)^2\right\}^{\frac{3}{2}}}e^{\frac{\delta'}{g}-g\theta_{2k}}d\theta_{2k},\\
&\psi_k^+=\delta'+\theta_{2k+1}+\Delta'+\frac{k\varepsilon_k\pi}{2},\\
&\psi_k^-=\delta'+\theta_{2k}-\Delta'-\frac{k\varepsilon_k\pi}{2},\\
&k=0,1,q=0,1.
\end{aligned} \tag{7.2}$$

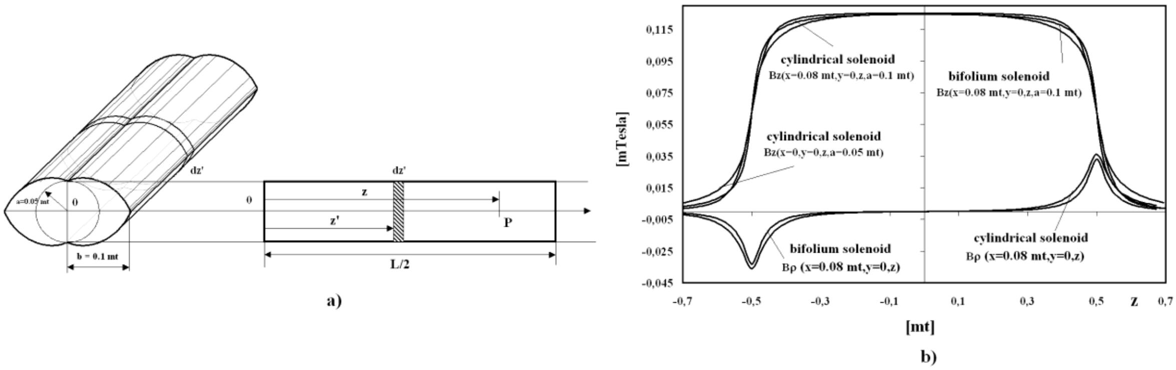

a)

b)

**Fig. (12). a**) perspective view and lateral view of the flat *bifolium* solenoid **b**) magnetic flux densities $B_z, B_\rho$ for the cylindrical and *bifolium* solenoids along z.

The contribution to the magnetic flux density at P along the z axis (x = 0, y = 0) of the *bifolium* solenoid is obtained analytically from Eq. (7.2), *i.e.*

$$B_{sol(2)z_{n,q}}\left(x=0,y=0,z\right)=$$
$$=\frac{\mu_0\mathbb{N}I}{\pi g}\ln\left[\frac{\sqrt{e^{2\frac{\delta'\left(1+g^2\right)}{g}-2g\left(n+\frac{1}{2}\right)\pi-qg\pi}+\left(z-\frac{L}{2}\right)^2}+z-\frac{L}{2}}{\sqrt{e^{2\frac{\delta'\left(1+g^2\right)}{g}-2g\left(n+\frac{1}{2}\right)\pi-qg\pi}+\left(z+\frac{L}{2}\right)^2}+z+\frac{L}{2}}\,\frac{\sqrt{e^{2\frac{\delta'\left(1+g^2\right)}{g}-2g\left(n+1\right)\pi-qg\pi}+\left(z+\frac{L}{2}\right)^2}+z+\frac{L}{2}}{\sqrt{e^{2\frac{\delta'\left(1+g^2\right)}{g}-2g\left(n+1\right)\pi-qg\pi}+\left(z-\frac{L}{2}\right)^2}+z-\frac{L}{2}}\right] \tag{7.3}$$

If the longitudinal dimension $L\gg e^{\frac{\delta'}{g}-g\theta_{2k}},e^{\frac{\delta'}{g}-g\theta_{2k+1}},\forall\theta_{2k},\theta_{2k+1}\in\left[-\delta'+n\pi+\frac{\pi}{2}+q\frac{\pi}{2},-\delta'+\left(n+1\right)\pi+\frac{\pi}{2}+q\frac{\pi}{2}\right]$, the magnetic flux density created by the *bifolium* solenoid becomes

$$B_{sol(2)z_{n,q}}\simeq\mu_0\mathbb{N}I \tag{7.4}$$

The solenoid *bifolium* creates the same uniform longitudinal magnetic flux density of the cylindrical solenoid, regardless of the values of n,q as shown in Fig. (**13**).

Examining in depth at the most significant differences between the *cylindrical* and the solenoid *bifolium*, it can be seen that, despite the magnetic flux densities obey to two different laws with the $f(z)=z/\sqrt{z^2+a^2}$ (see for example [31]) and $g(z)=\ln\sqrt{z^2+a^2}$ (see Eq. (7.3)) functions respectively, the results for the long sections L coincide. Moreover, the transverse components of the *bifolium solenoid* are small with respect to the longitudinal $B_z$ component (see Fig. **10** for the single loop coil).

The case of *multi-bifolium* is slightly different because Eq. (7.2) must be integrated between $-\delta'+n_0\pi+\frac{\pi}{2}$ and $-\delta'+n_0\pi+M\pi+q\frac{\pi}{2},M,n_0\in\mathbb{N}$

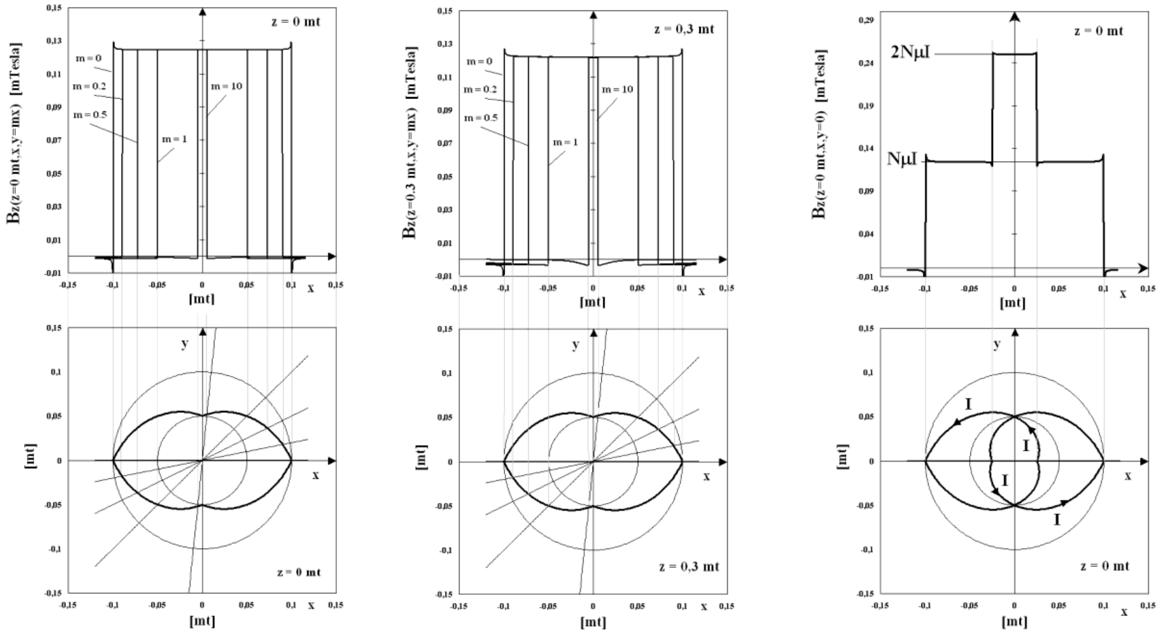

**Fig. (13).** $B_z$ of the *bifolium* solenoid as a function of x and y = mx at **a)** *z*=0 mt and **b)** *z*=0.3 *m*t, **c)** magnetic flux $B_z$ of a *multibifolium* solenoid $(n_0=0,M=1,q=1)$ resulting from two nested solenoids (q = 0 and q = 1), as a function of x at y = 0 and z = 0.

Again, using the superposition principle, the longitudinal magnetic flux density within the innermost *bifolium* coil results

$$B_{sol(2)z_{n,q}} \simeq 2\left(M - n_0\right)\mathbb{N}I \tag{7.5}$$

The case of two nested *bifolium* solenoids is represented in Fig. (**13c**).

## 8. THE SPIRAL *FOUR LEAF CLOVER* AND THE $2^p$ CROWN SOLENOIDS.

From the union of two *bifolium* coils one rotated with respect to the other by an angle $\pi/2$, the closed loop coil called spiral *four leaf clover* of Fig. (**14a**).

The same concept is generalized to the $2^p$ leaves coil of Fig. (**14b**) (p = 4).

The equations of the $2^p$ *forward* → and *backward* ← coil-parts are

$$\begin{gathered}
(2k)\leftarrow\begin{cases} x = -e^{\frac{\delta_{2k}}{g} - g\theta_{2k}}\cos\left(\delta_{2k} + \theta_{2k} - \Delta' - \dfrac{k\varepsilon_k\pi}{2^p}\right), \\ y = e^{\frac{\delta_{2k}}{g} - g\theta_{2k}}\sin\left(\delta_{2k} + \theta_{2k} - \Delta' - \dfrac{k\varepsilon_k\pi}{2^p}\right), \end{cases} \\
\theta_{2k} \in \left[-\delta_{2k} + n\pi + \frac{\pi}{2} + q\frac{\pi}{2^p}, -\delta_{2k} + \left(n+1\right)\pi + M\frac{\pi}{2} + q\frac{\pi}{2^p}\right], \\
(2k+1)\leftarrow\begin{cases} x = e^{\frac{\delta_{2k+1}}{g} - g\theta_{2k+1}}\cos\left(\delta_{2k+1} + \theta_{2k+1} + \Delta' + \dfrac{k\varepsilon_k\pi}{2^p}\right), \\ y = e^{\frac{\delta_{2k+1}}{g} - g\theta_{2k+1}}\sin\left(\delta_{2k+1} + \theta_{2k+1} + \Delta' + \dfrac{k\varepsilon_k\pi}{2^p}\right), \end{cases} \\
\theta_{2k+1} \in \left[-\delta_{2k+1} + n\pi + \frac{\pi}{2} + q\frac{\pi}{2^p}, -\delta_{2k+1} + \left(n+1\right)\pi + M\frac{\pi}{2} + q\frac{\pi}{2^p}\right], \\
k = 0,1,2,\ldots 2^p - 1, \delta_{2k} = \delta_{2k+1} = \delta' = \delta'' = const.
\end{gathered} \tag{8.1}$$

where $(2k)$, $(2k+1)$, are the subsets of the plane $\mathbb{R}^2$ that represent the boundaries of the $n^{th}$ *crown* coil. The integer $p \in \mathbb{N}$ represents the number of leaves $2^p$ of the *crown* coil (see Fig. **14c**), q represent the starting nested *crown* coil between n and n + 1 considered and M is the number of superimposed loops (M = 1, single loop see Fig. **14a** and Fig. **14b**).

The magnetic flux density created by the *crown* coil identified by the $\left(n, 2^p, q, M\right)$ numbers is given by

$$\begin{aligned}
&\vec{B}_{\left(n,2^p,q,M\right)}\left(\overrightarrow{r_p},\delta'=\delta'',\Delta',\bigcirc_{\uparrow}\right)=\vec{B}_{\left(n,2^p,q,M\right)}\left(\overrightarrow{r_p},\Delta',\rightarrow\right)+\vec{B}_{\left(n,2^p,q,M\right)}\left(\overrightarrow{r_p},-\Delta',\leftarrow\right)=\\
&=\frac{\mu_0 I}{4\pi}\sum_{k=0}^{2^p-1}\int_{-\delta'+n\pi+\frac{\pi}{2}+q\frac{\pi}{2^p}}^{-\delta'+n\pi+\frac{\pi}{2}+M\frac{\pi}{2^p}+q\frac{\pi}{2^p}}\frac{\left\{\begin{array}{l} z\left(-g\sin\left(\psi_k^+\right)+\cos\left(\psi_k^+\right)\right)\hat{e}_x+z\left(g\cos\left(\psi_k^+\right)+\sin\left(\psi_k^+\right)\right)\hat{e}_y+\\ +\left[e^{\frac{\delta'}{g}-g\theta_{2k+1}}-x\left(-g\sin\left(\psi_k^+\right)+\cos\left(\psi_k^+\right)\right)-y\left(g\cos\left(\psi_k^+\right)+\sin\left(\psi_k^+\right)\right)\right]\hat{e}_z\end{array}\right\}}{\left\{\left(x-e^{\frac{\delta'}{g}-g\theta_{2k+1}}\cos\left(\psi_k^+\right)\right)^2+\left(y-e^{\frac{\delta'}{g}-g\theta_{2k+1}}\sin\left(\psi_k^+\right)\right)^2+z^2\right\}^{\frac{3}{2}}}e^{\frac{\delta'}{g}-g\theta_{2k+1}}d\theta_{2k+1}+\\
&+\frac{\mu_0 I}{4\pi}\sum_{k=0}^{2^p-1}\int_{-\delta'+n\pi+\frac{\pi}{2}+q\frac{\pi}{2^p}}^{-\delta'+n\pi+\frac{\pi}{2}+M\frac{\pi}{2^p}+q\frac{\pi}{2^p}}\frac{\left\{\begin{array}{l} z\left(g\sin\left(\psi_k^-\right)-\cos\left(\psi_k^-\right)\right)\hat{e}_x+z\left(g\cos\left(\psi_k^-\right)+\sin\left(\psi_k^-\right)\right)\hat{e}_y+\\ +\left[e^{\frac{\delta'}{g}-g\theta_{2k}}+x\left(-g\sin\left(\psi_k^-\right)+\cos\left(\psi_k^-\right)\right)-y\left(g\cos\left(\psi_k^-\right)+\sin\left(\psi_k^-\right)\right)\right]\hat{e}_z\end{array}\right\}}{\left\{\left(x+e^{\frac{\delta'}{g}-g\theta_{2k}}\cos\left(\psi_k^-\right)\right)^2+\left(y-e^{\frac{\delta'}{g}-g\theta_{2k}}\sin\left(\psi_k^-\right)\right)^2+z^2\right\}^{\frac{3}{2}}}e^{\frac{\delta'}{g}-g\theta_{2k}}d\theta_{2k},\\
&\psi_k^+=\delta'+\theta_{2k+1}+\Delta'+\frac{k\varepsilon_k\pi}{2},\\
&\psi_k^-=\delta'+\theta_{2k}-\Delta'-\frac{k\varepsilon_k\pi}{2},\\
&k=0,1,q=0,1.
\end{aligned}\tag{8.2}$$

According to Eq. (8.2), for $x=0,y=0$ the magnetic flux density x-y-components created by the crown coil along the axis $z\neq 0$ are $B_x\left(n,2^p,q,M\right)=B_y\left(n,2^p,q,M\right)=0$ and, the z component is a generalization of Eq. (6.3), i.e.

$$B_{\left(2^p\right)z_{n,q,M}}\left(x=0,y=0,z\right)=\frac{\mu_0 I 2^{p-1}}{\pi g}\left[\frac{1}{\sqrt{e^{2\frac{\delta'\left(1+g^2\right)}{g}-2g(n+1)\pi-q\frac{g\pi}{2^{p-1}}}+z^2}}-\frac{1}{\sqrt{e^{2\frac{\delta'\left(1+g^2\right)}{g}-2g\left(n+\frac{1}{2}\right)\pi-q\frac{g\pi}{2^{p-1}}-M\frac{g\pi}{2^{p-1}}}+z^2}}\right]\tag{8.3}$$

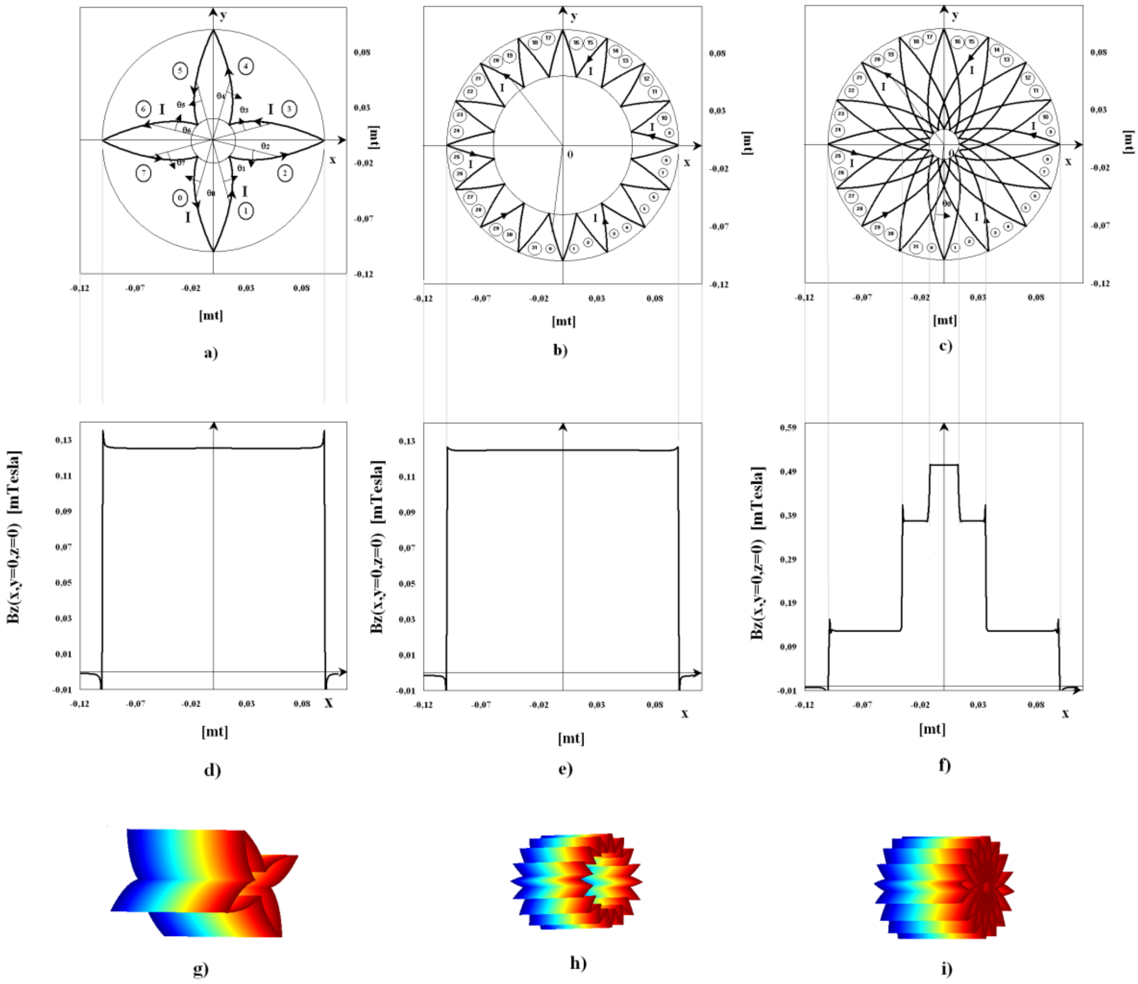

**Fig. (14). a)** and **g)** *four leaf clover* coil (p=2,M=1,q=0) **b)** and **h)** *crown* solenoid (p=4,M=1,q=0) **c)** and **i)** *crown* (p=4,M=4,q=0), **d)** and **e)** , **f)** Bz *versus* x at y = 0, z = 0 *four leaf clover*, *crown* solenoids, **g)** and **h)** , **i)** figures were obtained by using MATLAB).

According to Eq. (7.1) and Eq. (8.2), the contribution to the magnetic flux density at P along the z axis $x=0, y=0$ for the single crown solenoid M = 1, is

$$B_{sol\left(2^p\right)z_{n,q,M=1}}\left(x=0,y=0,z\right)=$$

$$=\frac{\mu_0 \mathbb{N} I 2^{p-1}}{\pi g}\ln\left[\frac{\sqrt{e^{2\frac{\delta'\left(1+g^2\right)}{g}-2g\left(n+\frac{1}{2}\right)\pi-\left(q+1\right)\frac{g\pi}{2^{p-1}}}+\left(z-\frac{L}{2}\right)^2}+z-\frac{L}{2}}{\sqrt{e^{2\frac{\delta'\left(1+g^2\right)}{g}-2g\left(n+\frac{1}{2}\right)\pi-\left(q+1\right)\frac{g\pi}{2^{p-1}}}+\left(z+\frac{L}{2}\right)^2}+z+\frac{L}{2}}\frac{\sqrt{e^{2\frac{\delta'\left(1+g^2\right)}{g}-2g\left(n+1\right)\pi-q\frac{g\pi}{2^{p-1}}}+\left(z+\frac{L}{2}\right)^2}+z+\frac{L}{2}}{\sqrt{e^{2\frac{\delta'\left(1+g^2\right)}{g}-2g\left(n+1\right)\pi-q\frac{g\pi}{2^{p-1}}}+\left(z-\frac{L}{2}\right)^2}+z-\frac{L}{2}}\right] \tag{8.4}$$

If the longitudinal dimension of the transverse ones, *i.e*

$L \gg e^{\frac{\delta'}{g}-g\theta_{2k}}, e^{\frac{\delta'}{g}-g\theta_{2k+1}}, \forall \theta_{2k}, \theta_{2k+1} \in \left[-\delta'+n\pi+\frac{\pi}{2}+q\frac{\pi}{2^p}, -\delta'+\left(n+1\right)\pi+\frac{\pi}{2}+\left(q+1\right)\frac{\pi}{2^p}\right]$, the magnetic flux density created by the *bifolium* solenoid becomes

$$B_{sol(2)z_{n,q,M=1}} \simeq \mu_0 \mathbb{N} I \tag{8.5}$$

## CONCLUSION

In this pioneering paper the designs of new spiral coils and solenoids have been presented. The theory is based on the *differential geometry of* the *phyllotaxis*, which consists in the use of the spiral orthogonal coordinates reflected and rotated to generate complex coil designs. Joining together two reflected spirals it is possible to obtain a loop whose shape resembles to that of a *leaf*. Detailed calculations of the electromagnetic fields created by the *leaf* loop were presented for both the static and the dynamic radiating antenna driven by a sinusoidal current $I(t)=A\cos(\omega t)$. Analytical expressions for magnetic flux density have been found for several spiral solenoid patterns. According to the limits for long solenoids, the inner magnetic flux density is uniform and directed along the z direction and proportional to the number of loops, exactly as for the cylindrical solenoid. Two advantages of the spiral solenoids with respect to the cylindrical solenoid are the possibility of obtaining the same uniform magnetic flux densities with the same current in a reduced space and of cooling them at low temperature by exploiting the holes between their coils.

Moreover, spiral coils may be used in specific applications of the space technology such as magnetic shields of spacecraft, space triaxial search coil magnetometers or to operate pistons and valves m of spacecraft. A countless number of new electromagnetic objects can be conceived through the use of the spiral coils and solenoids, whose versatility may be exploited to fit specific geometrical needs.

## References

[1] E. Waffenschmidt,Wireless power for mobile devices, *Telecommunications Energy Conference (INTELEC), 33$^{rd}$ International IEEE*, 2011.

[2] H. Lenz, Ueber die Bestimmung der Richtung der durch elekrodynamische Vertheilung erregten galvanischen Ströme, *Annalen der Physik und Chemie*, vol. 31, pp. 483, 1834.

[3] N. Tesla, Coil for electro magnets, *Patent no.* 512, 340, Jan 9, 1894.

[4] M. S. Karoul *et al*., Study and design of a loop antenna for medical telemetry application, *Sensors, Circuits & Instrumentation Systems Third International Conference on System, Signals & Devices March, Sousse, Tunisia, Vol. IV*, pp. 21-24, 2005.

[5] T.K. Sarkar *et al*., History of Wireless, *John Wiley &Sons*, 2006

[6] L.M.B. Campos and P.J.S.Gil, On spiral coordinates with application to wave propagation, *J. Fluid Mech., Cambridge University Press*, vol. 301, pp. 153-173, 1995.

[7] I.M.Fabbri,The Spiral Coaxial Cable, *International Journal of Microwave Science and Technology* Hindawi Pub. Corp., 2015.

[8] E.M Wassermann, C. M. Epstein, U. Ziemann, V. Walsh, T. Paus, The Oxford Handbook of Transcranial Stimulation, *Oxford University Press*, 2008.

[9] A.Maravita, N. Bolognini, Updates on multisensory perception: from neurons to cognition, *Frontiers Media SA e-book*, 2012.

[10] L.G. Cohen *et al*., Effects of coil design on delivery of focal magnetic stimulation. Technical considerations, *Electroencephalography and clinical Neurophysiology*, Elsevier pub., vol. 75, pp. 350-357, 1990.

[11] G. Xu *et al*., The Optimal Design of Magnetic Coil in Transcranial Magnetic Stimulation, *Proc. of the 2005 IEEE Engineering in Medicine and Biology 27th Annual Conference* Shanghai, China, September, pp.1-4, 2005.

[12] V. Kuperman, MRI, Physical principles and applications, *Academic Press*, 2000.

[13] Raja Parasuraman, M. Rizzo, Neuroergonomics: The Brain at Work: The Brain at Work, *Oxford University Press*, USA, 2006

[14] P. R. Troyk, G.A. DeMichele, D.A. Kerns, R.F. Weir, IMES: An Implantable Myoelectric Sensor, *Proceedings of the 29th Annual International Conference of the IEEE EMBS*, Lyon, France, 2007.

[15] R. Melik, N. K. Perkgoz, E. Unal, C. Puttlitz and H. V. Demir, Bio-implantable passive on-chip RF-MEMS strain sensing resonators for orthopaedic applications, *J. Micromech. Microeng.* vol. 18 pp. 115017, 2008.

[16] R.N. Simons, D.G.Hall, and F. A. Miranda, Spiral Chip Implantable Radiator and Printed Loop External Receptor for RF Telemetry in Bio-Sensor Systems, *NASA/TM*-2004-213217.

[17] R. Bancroft, Microstrip and Printed Antenna Design, *Noble Publishing*, 2004.

[18] J.M. Schelmann, Multi-user MIMO-OFDM in Practice Enabling Spectrally Efficient Transmission Over Time varying Channels, *Südwestdeutscher Verlag*, 2009.

[19] C.A. Kleitzing, ”The Electric and Magnetic Field Instrument Suite and Integrated Science (EMFISIS) on RBSP”, Space Sci. Rev., Springer, vol. 179, pp. 127-181, 2013.

[20] S. Tumanski, Induction Coil Sensors - a Review, *Meas. Sci. Technol., IOP publishing group*, vol. 18, pp. R31 R46,2007.

[21] A. Roux, The Search Coil magnetometer for THEMIS, *Space Science Reviews* vol.141, iss. 1, pp. 265-275, dec.2008.

[22] B.Romanowicz, A. Dziewonski, ”Treatise on Geophysics”, Elsevier, 2015.

[23] D.Cohen E.Halgren, Magnetoencephalography, in G. Adelman, B. Smith *Encyclopedia of Neuroscience*, Elseviers, 2004.

[24] J.C.Lin, Electromagnetic Fields in Biological Systems, *CRC*, 2011.

[25] J.H.Schultz, T. Antaya, J. Feng, C.Y.Gung, N. Martovetsky, J.V.Minervini, P. Michael, A. Radovinsky, P. Titus, The ITER Central Solenoid, Fusion Engineering, *Twenty-First IEEE/NPS Symposium on*, 2005

[26] P. Vedrine, Large Superconducting Magnet systems, *CERN Yellow Report* CERN-2014-005, pp. 559-583, 2014.

[27] R. Battiston *et al.*, Active Radiation Shield for Space Exploration Missions, ARSSEM, *Final Report ESTEC* Contract Nr. 4200023097/10/NL/AF, 2012.

[28] S. Tumanski, Handbook of Magnetic Measurements, *CRC Press*, 2011

[29] N. K. Das, P. Barat, S. Dey and T. Jayakumar , Design of Miniature Coil to Generate Uniform Magnetic Field, *Progress In Electromagnetics Research* M, Vol. 34, 99-105,2014.

[30] R. Beck, Magnetic fields in the nearby spiral galaxy IC342: A multi-frequency radio polarization study, A&A, 578, A93, 2015.

[31] J. D. Jackson, Classical electrodynamics, *John Wiley & Sons*, Inc. New York, Sydney, London, 1962

[32] G Arfken, University Physics, *Academic Press*, 2012.

[33] D.J. Griffiths, Introduction to Electrodynamics, *Prentice Hall* New Jersey 3rd. ed., 1999.

[34] N. Derby, S. Olbert, Cylindrical Magnets and Ideal Solenoids, *American Journal of Physics*, vol. 78, pp. 229 235, 2010.